HERMETIC IMPLANTABLE ANTENNA INSIDE VITREOUS HUMOR SIMULATING FLUID

H. Permana, Q. Fang*, and W. S. T. Rowe

School of Electrical and Computer Engineering, RMIT University, Melbourne, VIC 3000, Australia

Abstract—Retinal prosthesis system is currently being developed in various places around the world. This system involved data transfer between an implanted antenna inside an eyeball and an external camera that is located just in front of the eyeball. While there are plenty of publications about the stimulating electrodes or the processing unit of the system itself, very limited amount has been published regarding the wireless communication link between the two antennas despite the fact that the electromagnetic wave will propagate through a complex medium in the form of Vitreous Humor. This paper will discuss about the constraints associated with implanting an antenna into an eyeball. An antenna design and simulation was performed with the aid of High Frequency Structure Simulator (HFSS) and its Finite Element Method (FEM) mathematical solver in the operating frequency of 402–405 MHz. The antenna, which was a 4 layer microstrip antenna, was positioned at the centre of a spherical model filled with homogeneous Vitreous Humor material. Antenna performances that include return loss, bandwidth, gain, radiation pattern, and SAR value are analysed and compared against those of other implantable antennas operating in Medical Implant Communication Service (MICS) band. Free space and simulating fluid measurements were also conducted on the fabricated antenna to validate the simulation results. It was concluded that the fabricated antenna was able to produce the similar performance to the simulation results and hence at the same level as the other antennas operating in material with lower dielectric constants and conductivities.

1. INTRODUCTION

Age-related Macular Degeneration (AMD) is a genetic disease that affects macula due to the damage in the retina and it can cause gradual visual impairments. In 2004, there were 1.75 million people who were diagnosed with AMD in USA [1] with the addition of 700,000 new patients annually [2]. Based on mathematical prediction [3], there will be 17.8 million prevalence of AMD by 2050. Retinitis Pigmentosa (RP) is another eye disease that could result in blindness and the incidence varies in different countries. In United States, it stands at 1 in 3700, while in Navajo Indians (native North America tribe), the incidence is as high as 1 in 1800 [2]. In these two cases, it was found that even though 95% of the photoreceptors are damaged, a great portion of bipolar and ganglion cells, which are responsible for transmitting signal to the brain, are still functional [4]. This is where a retinal prosthesis system comes into the picture.

Retinal prosthesis is a prosthetic device aimed to help restoring partial vision of people who suffer from RP and AMD by using two separate components, an external camera and an internal array of electrodes for retina stimulation. The external camera is attached to spectacles or goggles in order to have the same projection as the eyeballs. This camera exchanges data wirelessly with the array of electrodes which is attached to the retina of the eye, inside the eyeball [5]. In this paper, the mechanism of the retinal prosthesis system will not be discussed, but the attention will be focused more to the intraocular antenna that receives the signal as well as transmitting telemetry signal back to the external device.

Designing an implantable antenna is a challenging task due to inevitable constraints that have to be considered, such as size, electrical characteristic of the surrounding materials, antenna material, as well as the Specific Absorption Rate (SAR) value limitation. Each part of human body has unique electrical characteristic, and the frequency dependability of each part makes it even more complicated. To satisfy the purpose of the antenna, Vitreous Humor was applied as the surrounding material in the simulation. Vitreous Humor is a semisolid gel structure inside an eyeball that is based on water (98%) and contains small amount of solid matters in the form of collagen, vitrosin, and hyaluronic acids [6]. Compared to other parts of human body, Vitreous Humor has a high relative permittivity and conductivity at 402 MHz ($\varepsilon_r = 69$, $\sigma = 1.5296$ S/m) [7], which makes it an inefficient medium for electromagnetic signal propagation. SAR is a regulatory threshold value to indicate safety operation level of any microwave emitter devices. According to the Institute of Electrical and Electronics

Engineers (IEEE) [8], SAR values on any 10 g average of tissues must not exceed 2 W/kg.

There have been substantial amount of research about implantable antenna design for various purposes such as biotelemetry [9], glucose monitoring [10], endoscopy [9], or retinal prosthesis system [11]. Single or multi-layer microstrip antenna was the most common geometry implemented in those systems due to its compact, robust, and simple and inexpensive characteristics. Numerical analyses were conducted either with mathematical tool like Matlab or with the aid of electromagnetic solvers like High Frequency Structure Simulator (HFSS), Computer Simulation Technology (CST), or *Feldberechnung bei Körpern mit beliebiger Oberfläche* (FEKO). At this stage, *in vivo* measurements for the purpose of simulation data validation are not feasible due to strict animal ethic regulations. The alternatives to the *in vivo* measurement include *in vitro* measurement using tissue mimicking fluid [9, 12, 13] or gel [14], measurement using minced pork [15, 16], or *in vivo* measurement using rats [17].

In this paper, an antenna was designed to be operative at 402–405 MHz Medical Implant Communication Service (MICS) band. With the aid of HFSS software, the antenna was designed and simulated inside two surrounding materials: free space and Vitreous Humor. The free space setup was investigated to provide reference for the free space measurement, while the immersion to the Vitreous Humor fluid was intended to accurately mimic the retinal prosthesis system. The presence of other eyeball parts such as sclera, lens, retina, etc. was not considered at this experiment due to lack of detailed 3D eyeball model available at this time. The electrical properties of those parts are slightly different compared to that of Vitreous Humor, with lower conductivities ($\sigma_{retina} = \sigma_{sclera} = 1$ S/m, $\sigma_{cornea} = 1.19$ S/m, $\sigma_{lens} = 0.67$ S/m) and lower dielectric constants ($\varepsilon_{r\,retina} = \varepsilon_{r\,sclera} = 57.66$, $\varepsilon_{r\,cornea} = 59.25$, $\varepsilon_{r\,lens} = 48.14$) [7]. The assumption that the whole spherical model is filled with only Vitreous Humor material would give worse result representation in comparison with the detailed model. Therefore, the use of plain Vitreous Humor sphere as the model is adequate at this stage in terms of getting the optimal performance out of the antenna.

At this stage, *in silico* measurement was performed with the aid of HFSS software. Data comparison and analysis was carried out with the aim of predicting the performance of the fabricated antenna. Comparisons were also made to other implantable antennas to set a benchmark for the proposed antenna. The proposed antenna was then fabricated and measured to obtain three different parameters: return loss, gain, and radiation pattern. The measurements were conducted

in three different configurations in order to closely monitor if the antenna indeed behaves in agreement to the simulation results. The conclusion at the end of this paper highlights the summary of the measured antenna performance against the simulation in terms of the three parameters.

2. ANTENNA DESIGNS

The fundamental geometry of the antenna was inspired by the multi-layer miniaturization technique proposed in [18]. The basic idea was to extend the conductor length as much as possible to compensate of low frequency operation without adding lateral dimensions. The antenna in [18] was designed for implementation inside skin simulating fluid, which at MICS band has a relative permittivity of 46.7 and conductivity of 0.69 S/m. A 3-layer antenna was initially designed and simulated by the author for the purpose of implantation inside the Vitreous Humor. However, the results were unsatisfactory with resonant frequency around 500 MHz and asymmetrical radiation pattern. A fourth layer of rectangular spiral conductor pattern was added on top of the same substrate material and height. The incorporation of the fourth layer was significant in lowering the resonance frequency as well as producing a more omnidirectional radiation pattern.

The proposed 4-layer microstrip antenna has a dimension of $10 \, \text{mm} \times 10 \, \text{mm} \times 2.54 \, \text{mm}$, with a shorting pin connecting the ground and the first layer. Material with high dielectric constant ($\varepsilon_r = 10.2$) was employed for the substrates, each with thickness of 0.635 mm (Figure 1(b)). The use of high dielectric constant material was aimed to realise smaller antenna dimension while preserving the antenna performance [19].

The first layer is ground layer, which is connected to the second layer by a ground pin and a feed pin. The second layer is a rectangular spiral microstrip and is connected to the third layer by the same feed pin that connects it to the first layer. And finally, the fourth layer is another rectangular spiral shaped antenna that acts as a director (Figure 1(c)). The use of multiple layers was intended to compensate the size constraint imposed on this antenna. This antenna was planned to be attached to an SMA coaxial connector for testing purpose. The coaxial and feed pin, as well as the connector arms, dimensions were made to match physical shape of R124.463.000 connector from Radiall, France.

An extra layer of polydimethylsiloxane (PDMS) was added to improve the characteristic of the antenna as well as providing
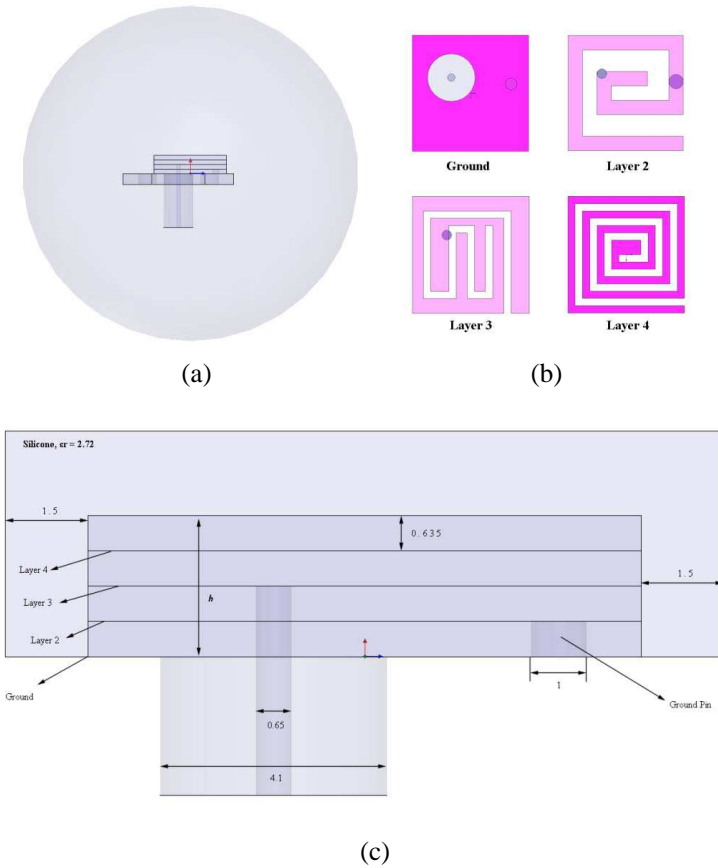
Figure 1. Antenna configuration, (a) inside the eyeball model, (b) the top view of each layer, and (c) from the side view with its silicone enclosure. All the units are in mm.

biocompatible characteristic to the antenna, which will help preventing any infections of the surrounding tissue in reaction to the implanted antenna. This extra layer encapsulates all the lateral sides as well as the top side of the antenna, which results in 1.5 mm longer at each side (Figure 1). The effect of this layer was investigated by applying various thicknesses on top of the antenna. This extra layer displaces what was actually the Vitreous Humor fluid, which is only positive to the simulation results due to the lower conductivity of the PDMS relative to the Vitreous Humor. The effect of the extra PDMS layer will be presented in the results section.

3. TISSUE MODELING

The antenna was designed to resemble the actual operation of the antenna inside a human eyeball. The antenna was simulated inside a spherical Vitreous Humor ($\varepsilon_r = 69$, $\sigma = 1.53\,\text{S/m}$ [20]). However, more simulations were executed with different configurations in order to accurately observe how the real antenna performs in relative to the simulation at 4 different set ups: an antenna in a free space sphere (Case A), an encapsulated antenna in a free space sphere (Case B), an encapsulated antenna in a Vitreous Humor sphere at the size of human eyeball (Case C), and an encapsulated antenna in a Vitreous Humor sphere at the size of table tennis ball (Case D). More information about the encapsulation would be available at the antenna design section.

The decision to use a simple eyeball model instead of a complex human head model for this study was based on the fact that the transmission between the intraocular and the extraocular parts always occur at the same unobstructed path from the inside to the distance of a few centimeters outwards the eyeball. This made the signal propagation analysis in that direction sufficed to obtain accurate representation of the antenna performance in respect to the system transmission. The presence of additional complex human head model would not affect the propagation in that particular direction.

Based on the simulation, Case C and Case D returned very similar results (look at Figure 2). Therefore, the utilization of table tennis ball, despite higher diameter (40 mm vs 25 mm), would still give an accurate representation on how the antenna will behave inside the real human eyeball. Special note to the spherical model in Case D, a thin layer of
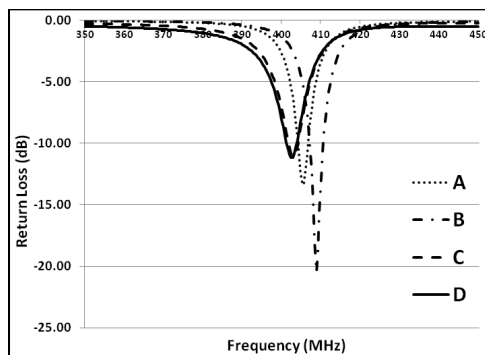
Figure 2. Return losses of the antenna in four different simulation setups. The letters A to D correspond to the Case A to Case D of the configuration.

celluloid (0.35 mm) was added, enclosing the Vitreous Humor sphere. The intention was to resemble the actual geometry of the table tennis ball in the real life.

4. SIMULATION RESULTS

The simulation data for different enclosure thickness (h) is presented in Table 1.

4.1. Return Loss

Based on the data on Table 1, the existence of PDMS enhanced return loss of the antennas. For the thinnest layer ($h = 3.05$ mm), an improvement of 3.31 dB was observed while 7.23 dB improvement was observed for the highest thickness simulated ($h = 4.06$ mm). According to this relationship, perpetual increment on the thickness would result in much better return loss property. However, space limitation will be an issue since the antenna will be implanted inside the eyeball that has typical diameter of 25 mm. Without the additional layer, the best return loss performance was -3.63 dB at 359.6 MHz, which is not good enough for reliable transmission.

Table 1. Antenna performance on different enclosure height.

h (mm)	frequency (MHz)	Return Loss (dB)	Max Gain (dB)	Efficiency
4.06	402.8	-10.86	-40.35	0.39%
3.81	401.6	-10.53	-40.3	0.39%
3.56	400.4	-9.99	-40.32	0.39%
3.3	398	-9.13	-40.34	0.38%
3.05	387.2	-6.94	-40.2	0.38%
0	359.6	-3.63	-43.5	0.17%

Table 2. Simulated antenna performance on different setups

Case	Frequency (MHz)	Min Return Loss (dB)	Max Gain (dB)	Efficiency
A	405.2	-13.28	-38.64	0.6%
B	408.8	-20.47	-38.5	0.6%
C	402.4	-10.86	-40.3	0.39%
D	402.4	-11.76	-39.4	0.46%

Based on the results on Table 1, the PDMS with the thickness of 4.06 mm was selected for further investigation involving the simulation of the antenna on free space. Figure 2 showed a comparison of the antenna return loss in the four different setups (Case A to Case D). As expected, shifts of resonance frequencies were evident for different setup with lower return losses present for free space surrounding material. This is due to the lossless property of the free space, in contrary to the lossy Vitreous Humor. These values will be used as the reference for the antenna measurements. More information about the antenna performance in four different cases can be observed on Table 2.

4.2. Max Gain and Radiation Pattern

The maximum simulated gains achieved by the antenna were in the region of -40 dB with the PDMS layer and -43.5 dB without the extra layer (Table 1). The presence of extra PDMS layer provided significant improvement to the antenna gain, but there was not much variation to the antenna gain when different extra layer heights were applied. From the result on Table 2, it can also be inferred that the addition of PDMS layer in free space did not affect the antenna gain performance. The immersion of the encapsulated antenna (Case C) degraded the gain by approximately 2 dB and the use of bigger eyeball size (Case D) produced a 1 dB improvement.

(a)   (b)
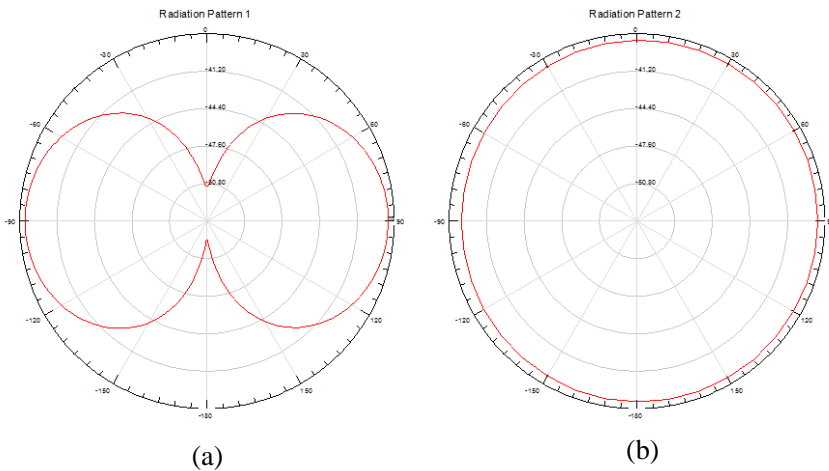
Figure 3. 2D Representation of simulated radiation pattern in (a) YZ plane, and (b) XY plane.

Table 3. Comparison of the proposed antenna against other published implantable antenna.

Antenna	Medium (ε_r, σ)	Gain (dB)
[12]	Skin Tissue (46.7, 0.69 S/m)	-37.96
[10]	Rat Skin (33, 0.5 S/m)	-27
[15]	Grinded Pork Leg (54, 0.8 S/m)	-27
[18]	2/3 Human Muscle (42.8, 0.65 S/m)	-38
Current	Vitreous Humor (69, 1.53 S/m)	-40.35

The radiation pattern is always omnidirectional regardless the presence of PDMS layer in any of the 4 cases, with the maximum values lie in x and y axis direction while the nulls occur at both end of the z-axis (Figure 3). This is a typical pattern of an electrically small antenna [20].

With this kind of radiation pattern, placing the antenna right in the middle of the sphere with the antenna facing upwards or downwards is the best possible set up since the signal will travel sideway, through to the external antenna. Since the interest is to deliver signal transmission in one direction ($+y$ axis), the gain in any other directions are ignored. A small shift in the direction of y-axis will improve the gain or the radiation efficiency.

The gain values of the antenna were very small compared to typical antenna gains due to the high conductivity characteristic of the Vitreous Humor ($\sigma = 1.53$ S/m) that inflicted losses to the signal propagation. There have not been any published experiments for implantable antenna inside a Vitreous Humor at MICS band, which makes it difficult to evaluate the gain performance of this antenna. The only possible way is to create a comparison with antennas implanted into muscle or skin materials ($\varepsilon_{r\,muscle} = 57.112 \sigma_{muscle} = 0.797$ S/m, $\varepsilon_{r\,skin} = 49.865 \sigma_{skin} = 0.67$ S/m [7]).

Table 3 is an aggregate of multiple published works on implantable antenna designs in various environments. It is clear that the proposed antenna lags behind the other listed antennas with the gap of 2 dB up to 13 dB. This discrepancy is due to the higher relative permittivity and conductivity value of the Vitreous Humor as the medium, which resulted in higher attenuation constant α. Attenuation constant is a signal attenuation associated to electromagnetic wave travelling in lossy medium where higher value indicates more signal loss during the

propagation. The relationship can be defined by Equation (1) [21].

$$\alpha = \omega\sqrt{\frac{\mu\varepsilon}{2}\left[1 + \frac{\sigma}{\varepsilon\omega} - 1\right]} \qquad (1)$$

with α is the attenuation constant (Np/m), μ is the permeability (H/m), ε is the permittivity (F/m), and σ is the conductivity (S/m).

Implementing this formula for different values of permittivity and conductivity gave a deeper comprehension about how both parameters affect the attenuation. Higher dielectric constant and/or higher conductivity result in higher attenuation constant. This explains an inclination to get lower gain when Vitreous Humor was implemented.

4.3. Radiation Efficiency

Radiation efficiency is closely related to the antenna gain and it can be represented by the following equation.

$$rad \cdot eff = \frac{P_{rad}}{P_{input}} \qquad (2)$$

where P_{rad} is the radiated power (W) and P_{input} is the power delivered to the antenna (W).

As presented in Table 1, the efficiency values obtained from the simulation were in the region of 0.38%–0.39% with the extra PDMS layer. The efficiency was reduced by a factor of 2 when the extra layer was removed. These values are considerably low compared to regular free space antenna. However, they are still comparable to the results of other published experiments by Liu (0.55%) [12], Lee (0.31%) [22], or Kim (0.25%) [13]. In all of those experiments, the antenna was simulated by using tissue or skin simulating fluid as the medium.

The antenna efficiency comparison in 4 different cases revealed that the introduction of PDMS layer in free space did not alter the efficiency. However, once the antenna was immersed inside the liquid (Case C), the efficiency degraded by 35%. A slight improvement on the efficiency was observed when a bigger eyeball size was utilized (Case D).

4.4. SAR

According to the HFSS simulation, the 10 g average SAR at the Vitreous cavity was 45 W/kg and 33 W/kg at Case C and Case D, respectively. The calculation was done under the condition that the input power to the antenna was 1 W. It means, to comply with the SAR safety limit of 2 W/kg, the input power should not exceed 44.4 mW and 60.6 mW for Cases C and D, respectively.

(a)   (b)
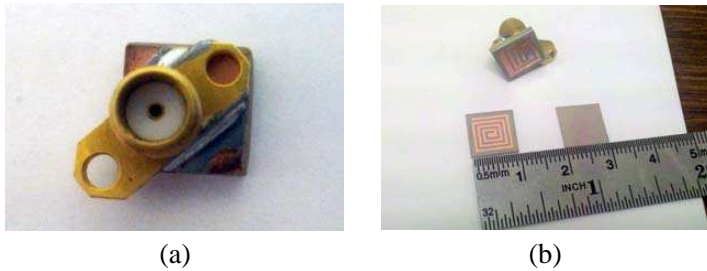
Figure 4. The image of the fabricated antenna seen (a) from the back with its SMA connector attached, and (b) on each layer separately before the adhesive material was applied.

5. ANTENNA FABRICATION

The fabrication of the antenna was done by the etching of each layer separately. The next step was drilling all the holes where the feed and ground pin will be placed. Accuracy on the drilling is highly prioritised since it greatly affects the feeding placement of the antenna. It is also critical that both pins do not extend beyond the conductor line to avoid excessive cross-polarized radiation [23]. When all the pins had been soldered, the rest of the substrates were stacked together and pressed with a vertical clamp. A layer of glue was then added to all 4 sides of the antenna to make sure that they stick together. The fabricated antenna can be seen on Figure 4.

The final phase of the antenna fabrication was the PDMS encapsulation to seal the antenna from the surrounding medium as well as providing biocompatibility characteristic. The process involved mixing PDMS gel with its diluents to adjust its flexibility as well as storing it in a high temperature (70°C) chamber to accelerate the hardening process. In the end, the PDMS layer was trimmed according to the specified width and length.

6. ANTENNA MEASUREMENT

The fabrication process of the antenna involved etching each RO3210 substrate, drilling specific diameter size holes and imbedding the corresponding pins, as well as stacking up all the layers together with adhesive material. Once fabricated, a series of measurements were undertaken on the antenna to obtain return loss, gain, and radiation pattern parameters. The return loss was measured with Agilent E5071B network analyzer, while the gain and radiation pattern measurement was conducted inside an anechoic chamber to ensure minimal level of unwanted reflections.
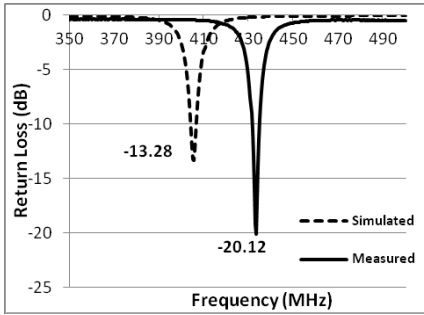
Figure 5. Return loss comparison between the simulation and the measurement results for Case A configuration.
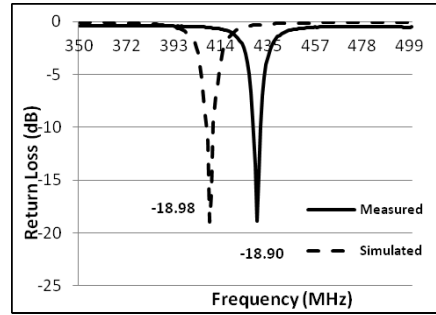
Figure 6. Return loss comparison between the simulation and the measurement results for Case B configuration.
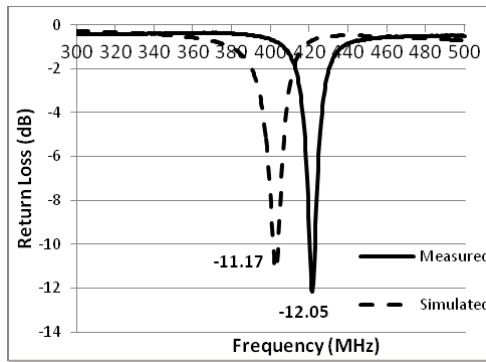
Figure 7. Return loss comparison between the simulation and the measurement results for Case D configuration.

Table 4. Measured antenna performance on different setups.

Case	Frequency (MHz)	Min. Return Loss (dB)
A	433.2	−20.12
B	430	−18.89
C	421.2	−12.05

6.1. Return Loss

Table 4 shows the measured return losses of the 3 cases, which were obtained with the aid of Agilent E5071B network analyser. It is apparent that there was a shift at the resonant frequencies on all three cases, ranging from 4.5% to 7% (Figures 5 to 7). Minor fabrication flaws that comprises of inaccurate pin placement, dimension inconsistency during the negative reproduction process, as well as the presence of adhesive material to the layers may contribute to this discrepancy.

6.2. Radiation Pattern

The measurement of the gain and the radiation of the antenna in all 3 cases were conducted inside an anechoic chamber. A half wave dipole antenna deputised as a source antenna and located at a distance such that both antennas are at each other's far field zone. This is to ensure that the AUT exposed to a plane wave of uniform amplitude, phase, and polarization [24]. The far field distance for both antenna was calculated using the following formula [25]:

$$R = \frac{2D^2}{\lambda} \qquad (3)$$

where D is the maximum aperture of the antenna, λ the wavelength, and R the far field distance. Based on this formula, the far field boundary of the dipole antenna and the antenna under test (AUT) were calculated to be 0.37 m and 0.27 mm, respectively. It implies that the minimum distance between the two antennas should be around 0.37 m to ensure far field transmission. The measurements were conducted inside a 6 m length anechoic chamber, which exceeds the required separation between the two antennas (Figure 8).

(a)	(b)
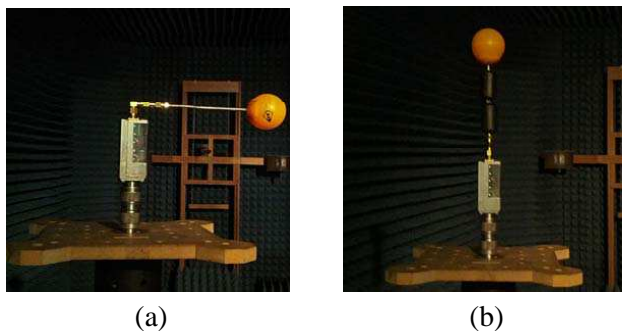
Figure 8. Measurement configuration of Case D on (a) vertical E-field, and (b) horizontal E-field inside an anechoic chamber.

The pattern measurement was carefully conducted with the guidance of IEEE Standard for Antenna Measurement [26] and its spherical coordinate system. Based on the model, 2 significant patterns were required, 360° rotation along the equator ($\varphi = 0°$ to 360°) at both $\theta = 0°$ and 90°. The equatorial rotation was controlled by a rotator with 450 data points acquired by the network analyser for every full 360° rotation. The 90° rotation of the θ was necessary to accommodate both horizontal and vertical E-field plane of the antenna. Those two patterns would contain enough information that represents the whole

Radiation Pattern Case A Horizontal

Radiation Pattern Case A Vertical

(a)

(b)
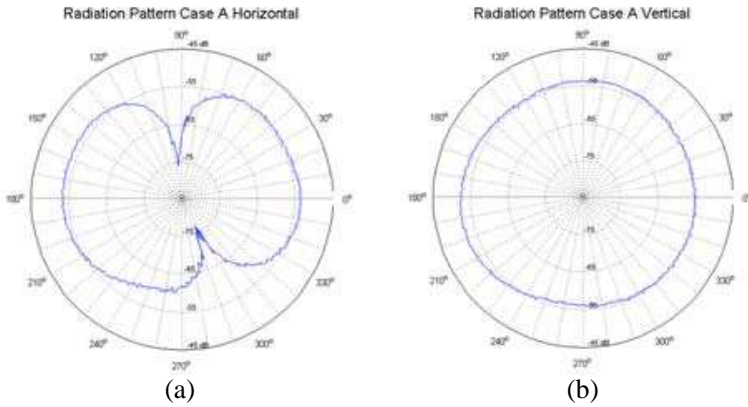
Figure 9. The radiation pattern of the antenna in Case A with (a) horizontal E-field, and (b) vertical E-field.

Radiation Pattern Case B Horizontal

Radiation Pattern Case B Vertical

(a)

(b)
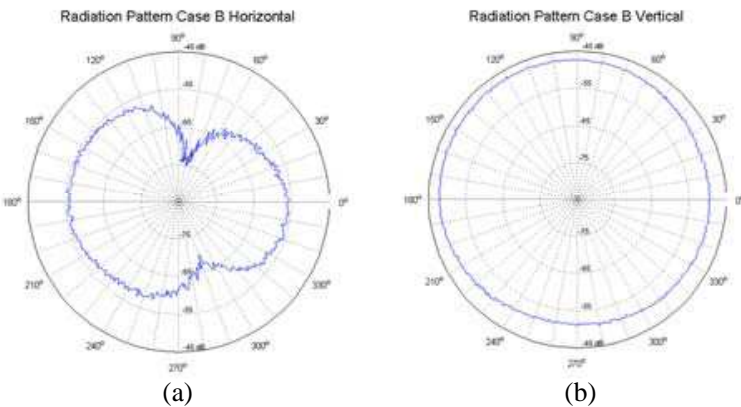
Figure 10. The radiation pattern of the antenna in Case B with (a) horizontal E-field, and (b) vertical E-field.
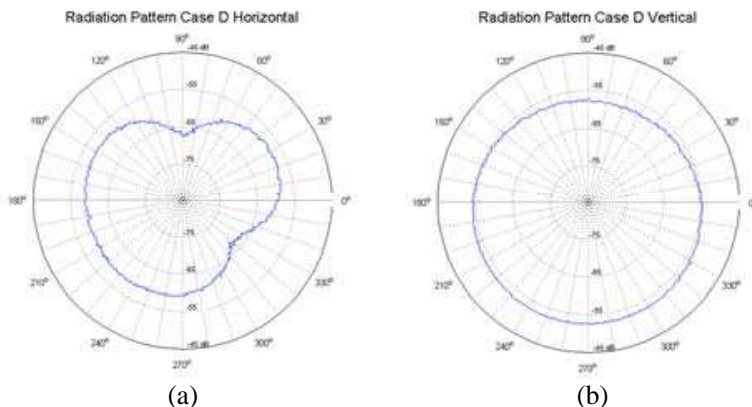
Figure 11. The radiation pattern of the antenna in Case D with (a) horizontal E-field, and (b) vertical E-field.

3D model by visually capturing all significant edges of the AUT.

Several testings were conducted prior to the real measurement to determine the polarization of the antenna. Based only on the simulation results, it was not clear which way the E-field of the antenna was propagating due to the spiral pattern at the layer 3 as well as the small feeding pin size. The E-field was finally determined to be propagating vertically, parallel to the pin and perpendicular to the antenna layers. With this knowledge, the measurement involving θ rotation can be done more precisely and the real pattern characteristic of the antenna can be captured.

Figures 9 to 11 showcased the measured radiation patterns inside the chamber. Figures 9(a), 10(a), and 11(a) visualised the co-polarization transmission when the E-field was travelling in vertical direction, while Figures 9(b), 10(b), and 11(b) showed the horizontal E-field transmission in 3 different cases. In terms of pattern shape, Figure 9 resembled the omnidirectional pattern observed from the simulation, with a pair of nulls observed around $\varphi = 90°$ and $\varphi = 270°$.

With the addition of PDMS layer, the basic pattern still looked the same, with the two nulls existed at the $\varphi = 90°$ (Figure 10). However, in this case, one of the lobes lost its gain and became moderately smaller than the other lobe. Just like previous case, the horizontal E-field pattern was a circular, which signified the omnidirectional characteristic of the antenna.

For the measurement of the last case (Case D), the same setup was used, only for the antenna was submerged inside a Vitreous Humor fluid filled table tennis ball (Figure 8). The table tennis ball was

modified such that the antenna was placed exactly at the centre of the ball, just as the simulation setup. The Vitreous Humor liquid was supplied by EMC Technologies, Melbourne, Australia, as a mixture of water, salt, and sugar with a characteristic of ε_r = 65.2 and σ = 1.59 S/m at 400 MHz and t = 22.1°C. The liquid was then injected through a small hole to fill the ball completely. The radiation pattern of this case can be observed on Figure 11. Here, the pattern still resembled the omnidirectional pattern, with the presence of two opposite nulls. However, as was observed at the previous case, one of the lobes was smaller than the other. This time, there was further degradation in terms of size of this shrinking lobe.

6.3. Gain

To calculate the gain of the antenna, the following formula was used:

$$G \text{ (dBi)} = G_{standard} + (G_{AUT} - G_{ref}) \tag{4}$$

where $G_{standard}$ is the known gain of the reference antenna (dBi), G_{AUT} is the measured gain of the tested antenna (dB), and G_{ref} is the measured gain of the reference antenna (dB). The reference antenna in this case was half wave dipole, which has a gain of 2.15 dBi. The significant points of gain from the measured radiation pattern were the ones at φ = 0° and φ = 180°. Those positions are where the highest gain should occur. Theoretically, those two points should overlap between the vertical and the horizontal E-field, but it is very hard to achieve a very exact pair in the real life due to a number of aspects. The calculation of the two points for all the cases can be seen on Table 5.

The data in Table 5 provide useful information about the antenna characteristic in terms of the radiation pattern and the gain values. Initially, it is important to look at the gain values of each antenna at φ = 0° and φ = 180° at one E-field direction and compare them against the gains of the same angle with another E-field direction. It is

Table 5. Measured gain of the antenna.

Case	Horizontal E-field		Vertical E-field	
Gain (dB)	$\Phi = 0°$	$\Phi = 180°$	$\Phi = 0°$	$\Phi = 180°$
A	−32.35	−32.17	−36.75	−33.84
B	−35.93	−36.07	−31.21	−30.09
D	−39.89	−39.29	−37.89	−37.36

evident that there are various discrepancies on the data with the range of 2 dB up to 6 dB. Possible contributing factors to the inconsistencies include alignment issues, non-symmetrical anechoic chamber, as well as spurious radiation from the coaxial cable.

Alignment mismatch is always an issue in measuring antenna in two different θ due to the ambiguous starting point of the rotation. However, the variations caused by this were not significant in relative to the gain values of the antenna. Non-symmetrical dimension of the room possibly created some unbalanced patterns that can be observed at Figures 10(b), 11(a), or 12(a). The nature of this measurement, which is low frequency, made it more difficult for an anechoic chamber to completely absorb all the unintended propagations. Some reflections, albeit small, may still present. They are even gaining their significances due to the low gain characteristic of the antenna. To minimize this problem, a symmetrical is required, to capture more balanced patterns of the antenna. Finally, all small antennas with limited ground plane are prone to spurious radiations from the coaxial cable. Diminishing this problem can be done by installing ferrite-core material along the coaxial cable. It would not eliminate the problem completely, but it made a more reasonable reading possible.

7. CONCLUSION

A novel 4-layer microstrip antenna simulated inside Vitreous Humor fluid has been proposed in this paper. The study has revealed a MICS Band implantable antenna for a retinal prosthesis system, which, to the authors' knowledge, has not been proposed previously. With a compact size of 13 mm × 12 mm × 4.06 mm (including the PDMS encapsulation), this antenna performed, *in silico*, at the same level as other published implantable antenna designs inside skin and muscle tissues despite more challenging conditions on the medium, Vitreous Humor. This substance has a relative permittivity of 69 and conductivity of 1.5296 S/m at 402 MHz, which are relatively high compared to the characteristic of other parts of the human body. It results in a higher attenuation constant in the signal propagation that translates into more signal loss.

It was proved that the addition of PDMS layer enhanced the performance of the antenna as well as solving the biocompatibility issue. Increasing the thickness of the extra layer inside the Vitreous Humor fluid improved the return loss characteristic of the antenna, but otherwise made little difference to the other parameters. It was decided that a thickness of 4.06 mm for the extra layer gave the best performance of the antenna without breaching any of the constraints.

The proposed antenna was designed and simulated using HFSS software in 4 different cases: A) an antenna in a free space sphere, B) an encapsulated antenna in a free space sphere, C) an encapsulated antenna in a Vitreous Humor sphere at the size of human eyeball, and D) an encapsulated antenna in a Vitreous Humor sphere at the size of ping pong ball. Each case was configured with the aim of better knowledge on the antenna behaviour. The simulation results demonstrated that the antenna could perform at similar level compared to other implantable antennas in less challenging environment.

The antenna was fabricated and measured in search of three different parameters: return loss, radiation pattern, and gain. Thorough tests were conducted and similar performances were obtained compared to the simulations. The return loss of the antenna in 3 different cases varied by 4.5% to 7%, while similar omni directional patterns were observed and the gain value of the Case D was precise.

The results were very satisfactory in respect to other similar documented experiments the next phase of this project includes *in vitro* or *in vivo* antenna testing, as well as integration of the antenna to the suitable microchip to build the complete system.

ACKNOWLEDGMENT

REFERENCES

1. Friedman, D. S., B. J. O'Colmain, B. Muñoz, S. C. Tomany, C. McCarty, P. T. V. M. De Jong, et al., "Prevalence of age-related macular degeneration in the United States," *Archives of Ophthalmology*, Vol. 122, No. 4, 564–572, 2004.

2. Margalit, E. and S. R. Sadda, "Retinal and optic nerve diseases," *Artificial Organs*, Vol. 27, No. 11, 963–974, 2003.

3. Rein, D. B., J. S. Wittenborn, X. Zhang, A. A. Honeycutt, S. B. Lesesne, and J. Saaddine, "Forecasting age-related macular degeneration through the year 2050: The potential impact of new treatments," *Archives of Ophthalmology*, Vol. 127, No. 4, 533–540, 2009.

4. Margalit, E., M. Maia, J. D. Weiland, R. J. Greenberg, G. Y. Fujii, G. Torres, et al., "Retinal prosthesis for the blind," *Survey of Ophthalmology*, Vol. 47, No. 4, 335–356, 2002.

5. Weiland, J. D., W. Liu, and M. S. Humayun, "Retinal prosthesis," *Annual Review of Biomedical Engineering*, Vol. 7, No. 1, 361–401, 2005, doi: 10.1146/annurev.bioeng.7.060804.100435.

6. Rogers, K., *The Eye: The Physiology of Human Perception,* Britannica Educational Publishing, Chicago, 2010, Available from: http://RMIT.eblib.com.au/patron/FullRecord.aspx?p=514090.

7. Gabriel, S., R. W. Lau, and C. Gabriel, "The dielectric properties of biological tissues: II. Measurements in the frequency range 10 Hz to 20 GHz," *Physics in Medicine and Biology*, Vol. 41, No. 11, 2251–2269, 1996.

8. Lin, J. C., "A new IEEE standard for safety levels with respect to human exposure to radio-frequency radiation," *IEEE Antennas and Propagation Magazine*, Vol. 48, No. 1, 157–159, 2006.

9. Kwak, S. I., K. Chang, and Y. J. Yoon, "Small spiral antenna for wideband capsule endoscope system," *Electronics Letters*, Vol. 42, No. 23, 1328–1329, 2006.

10. Karacolak, T., R. Cooper, and E. Topsakal, "Electrical properties of rat skin and design of implantable antennas for medical wireless telemetry," *IEEE Transactions on Antennas and Propagation*, Vol. 57, No. 9, 2806–2812, 2009.

11. Soora, S., K. Gosalia, M. S. Humayun, and G. Lazzi, "A comparison of two and three dimensional dipole antennas for an implantable retinal prosthesis," *IEEE Transactions on Antennas and Propagation*, Vol. 56, No. 3, 622–629, 2008.

12. Liu, W. C., S. H. Chen, and C. M. Wu, "Bandwidth enhancement and size reduction of an implantable PIFA antenna for biotelemetry devices," *Microwave and Optical Technology Letters*, Vol. 51, No. 3, 755–757, 2009.

13. Kim, J. and Y. Rahmat-Samii, "Implanted antennas inside a human body: Simulations, designs, and characterizations," *IEEE Transactions on Microwave Theory and Techniques*, Vol. 52, No. 8, 1934–1943, 2004.

14. Karacolak, T., A. Z. Hood, and E. Topsakal, "Design of a dual-band implantable antenna and development of skin mimicking gels for continuous glucose monitoring," *IEEE Transactions on Microwave Theory and Techniques*, Vol. 56, No. 4, 1001–1008, 2008.

15. Lee, C. M., T. C. Yo, F. J. Huang, and C. H. Luo, "Bandwidth

enhancement of planar inverted-F antenna for implantable biotelemetry," *Microwave and Optical Technology Letters,* Vol. 51, No. 1, 749–752, 2009.

16. Huang, F. J., C. M. Lee, C. L. Chang, L. K. Chen, T. C. Yo, and C. H. Luo, "Rectenna application of miniaturized implantable antenna design for triple-band biotelemetry communication," *IEEE Transactions on Antennas and Propagation*, Vol. 59, No. 7, 2646–2653, 2011.

17. Karacolak, T., R. Cooper, J. Butler, S. Fisher, and E. Topsakal, "In vivo verification of implantable antennas using rats as model animals," *IEEE Antennas and Wireless Propagation Letters*, Vol. 9, 334–337, 2010.

18. Liu, W. C., F. M. Yeh, and M. Ghavami, "Miniaturized implantable broadband antenna for biotelemetry communication," *Microwave and Optical Technology Letters*, Vol. 50, No. 9, 2407–2409, 2008.

19. Soontornpipit, P., C. M. Furse, and Y. C. Chung, "Design of implantable microstrip antenna for communication with medical implants," *IEEE Transactions on Microwave Theory and Techniques*, Vol. 52, No. 8, 1944–1951, 2004.

20. Balanis, C. A., *Antenna Theory,* 3rd Edition, John Wiley & Sons, Inc., New Jersey, 2005.

21. Ulaby, F. T., *Fundamentals of Applied Electromagnetics,* 5th Edition, 464, Pearson Education, Inc., Upper Saddle River, 2007.

22. Lee, C. M., T. C. Yo, C. H. Luo, C. H. Tu, and Y. Z. Juang, "Compact broadband stacked implantable antenna for biotelemetry with medical devices," *Electronics Letters*, Vol. 43, No. 12, 660–662, 2007.

23. Waterhouse, R. B., *Microstrip Patch Antennas: A Designer's Guide,* Kluwer Academic Publishers, Boston, 2003.

24. Blake, L. V. and M. W. Long, *Antennas — Fundamentals, Design, Measurement,* 3rd Edition, 371–421, SciTech Publishing, 2009.

25. Johnson, R. C., *Antenna Engineering Handbook,* 3rd Edition, McGraw-Hill, Inc., New York, 1993.

26. IEEE, *IEEE Standard Test Procedures for Antennas,* Wiley-Interscience, 1979.